ADVANCED OPTICAL MATERIALS
www.advopticalmat.de

Phase-Shifted Bragg Gratings from High Refractive Index Chalcogenide Hybrid Inorganic/Polymers: Fabrication and Thermo-Optic Characterization

Abhinav Nishant, Kyung-Jo Kim, Roland Himmelhuber, Taeheon Lee, Tristan S. Kleine, Jeffrey Pyun, and Robert A Norwood**

In this study, the first fabrication of phase-shifted Bragg gratings utilizing chalcogenide hybrid inorganic/organic polymers (*CHIPs*) is presented based on poly(sulfur-*random*-(1,3-isopropenylbenzene) to measure the thermo-optic coefficient (TOC) of this new class of optical polymers. The unique properties of *CHIPs*, such as high index contrast and low optical losses, are leveraged to fabricate Bragg gratings that enable precise determination of the TOC and glass transition temperature (T_g) of these polymers. The optical measurement introduces a novel technique to measure the TOC and T_g of optical polymers which can be difficult to determine using traditional methods such as differential scanning calorimetry (DSC) after fabrication into photonic device constructs. The findings demonstrate that *CHIPs* exhibit low thermo-optic (TO) effects, making them exceptionally well-suited for the development of thermally stable photonic integrated circuits.

1. Introduction

Polymer-based photonic integrated circuits have been gaining interest in recent years.[1–4] With industrial and academic interest rising for applications like augmented reality/virtual reality (AR/VR),[5,6] light detection and ranging (LIDAR),[7] and on-chip sensors,[8] optical polymers offer a scalable and robust platform for mass-producing devices for many of these commercial applications. With novel chemistry and innovative reaction strategies, optical polymers can be synthesized with widely tunable properties, leading to mass-produced optical devices at lower costs. While the polymer community has devoted significant effort to synthesizing robust optical polymers, there also needs to be an equal drive from the photonics community to utilize these polymers for superior photonic integrated circuit (PIC) devices. Additionally, the material properties of these new materials need to be better understood. Compared to silicon photonics, polymer PICs traditionally suffer from low index contrast, higher optical losses, and higher TO coefficients limiting their applications for making some high-performance devices; notable exceptions are TO variable attenuators, phase shifters, and switches. Hence, in general, there is a need for optical polymers and polymer devices with higher indices, low thermo-optic coefficients, and lower optical absorption losses which provide viable alternatives to silicon nitride and other commonly used integrated optics materials.

We previously demonstrated our progress in solving some of these issues by fabricating passive photonic components using chalcogenide hybrid inorganic/organic polymers (*CHIPs*) as the core material platform. *CHIPs* have been developed as a high index, low loss optical polymer with highly desirable optical properties for a broad wavelength range from the shortwave to mid-wave infrared (IR) wavelengths.[9–12] These polymers can be manufactured and processed at a fraction of the cost required for chalcogenide glasses, silicon nitride, lithium niobate, etc. due to their chemical composition and facile processing capabilities. This suite of unique and favorable optical properties was leveraged for the first fabrication of integrated photonic components using our first-generation *CHIPs* materials with poly(sulfur-*random*-(1,3-diisopropenylbenzene))(poly(S-*r*-DIB). The production of single-mode photonic devices using high index poly(S-*r*-DIB) as the high refractive index (RI) core material for the fabrication of polymer waveguides, splitters, and high Q-high finesse ring resonators was demonstrated via an electron beam lithographic process;[13] we note that processes based on optical lithography have also been developed. This work demonstrated the viability of CHIPs as a new class of polymers for *integrated photonics* that exhibit excellent optical waveguide performance and record reductions in device feature size, particularly for polymeric ring resonators, as integrated photonic elements in functioning devices. These findings highlighted the benefits of the high RI and low optical losses of these materials, with waveguides fabricated using conventional lithography

A. Nishant, K.-J. Kim, R. Himmelhuber, R. A Norwood
J. C. Wyant College of Optical Sciences
University of Arizona
Tucson, AZ 85721, USA
E-mail: rnorwood@optics.arizona.edu
T. Lee, T. S. Kleine, J. Pyun
Department of Chemistry and Biochemistry
University of Arizona
Tucson, AZ 85721, USA
E-mail: jpyun@arizona.edu

The ORCID identification number(s) for the author(s) of this article can be found under https://doi.org/10.1002/adom.202401296

DOI: 10.1002/adom.202401296

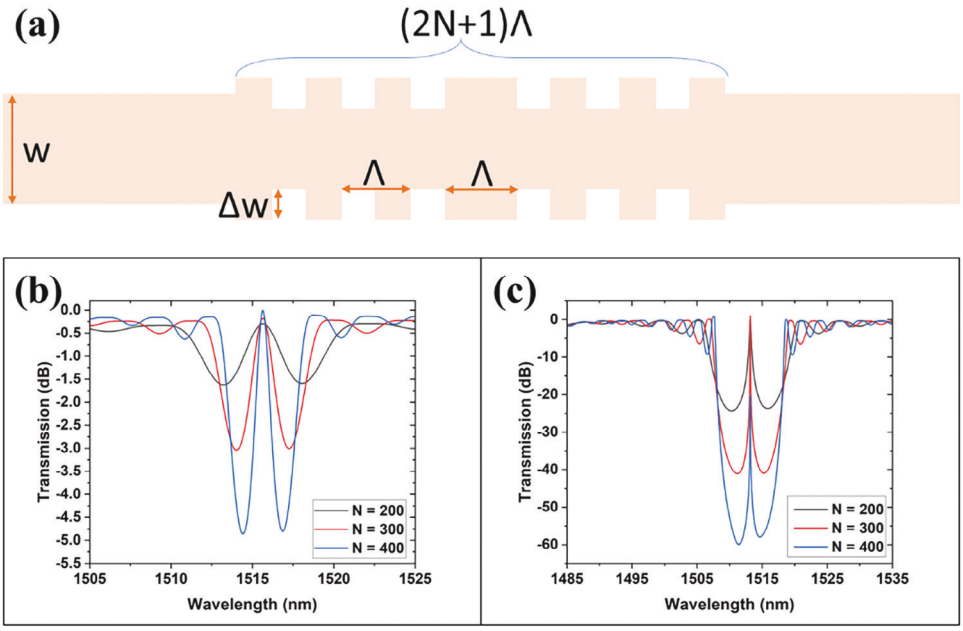

Figure 1. a) Schematic of the PSBG integrated with a single-mode waveguide of width, w = 1.5 μm. The grating has a period given by Λ, a width corrugation of Δw, and a quarter-wave phase shift region with a length equal to Λ. The total length of the grating region is (2N + 1)Λ, where N is the number of gratings on each side of the phase shift region. b) EME model of the grating transmission for Δw = 100 nm, for N equal to 200, 300, and 400. c) EME model of the grating transmission for Δw = 250 nm, for N equal to 200, 300, and 400.

techniques. These advantages in conjunction with the low cost of these optical polymers due to the use of elemental sulfur point to the potential for scaling up the fabrication to wafer-level processes in realizing all-polymer photonic devices. In this work, we further expand on our work by demonstrating the first fabrication of high index contrast phase-shifted Bragg gratings (PSBG), where the high sulfur content and high RI of *CHIPs* afford device components with narrow linewidths and high transmission. The PSBG's are a particularly useful photonic device construct to enable tunable filtering for telecommunication applications by appropriate design of the polymer grating dimensions. To highlight our capabilities further, we have utilized the gratings for fundamental polymer physical studies, specifically to interrogate the thermo-optic behavior of *CHIPs*, which previously has not been reported. We also introduce this technique as a novel optical method for determining the glass transition temperature (T_g) of new polymers targeted at thin-film applications, particularly during *in operando* device constructs, where the bulk versus thin-film thermal properties can significantly differ. We observe in this study that poly(S-*r*-DIB) has significantly lower TO effects compared with traditional optical polymers, coupled with very low materials/fabrication costs making them suitable for manufacturing thermal drift-resistant PICs.

1.1. Design of Phase-Shifted Bragg Gratings from High RI poly(S-r-DIB)

Bragg gratings have been integrated with planar single-mode waveguides using poly(S-*r*-DIB) as the core material platform, where the index modulation in the grating arises from the corrugation of the width of the waveguide.[14] The corrugation is defined by $w \pm \Delta w$, where w is the width of the waveguide and Δw is the variation in the width in the grating region of the waveguide (**Figure 1a**). We also vary the grating periodicity to study the grating response to the linewidth of the Bragg peak. To analyze the grating response, we modeled the single-mode conditions using Lumerical MODE software. Finite difference eigenmode (FDE) and eigenmode expansion (EME) solvers were used to obtain the waveguide modal properties and grating response, respectively. We initially modeled the waveguide cross-section with width, w = 1.5 μm, and height, h = 0.45 μm. The refractive index of the core material is 1.74 at 1550 nm and was measured using the Metricon prism coupling instrument, employi silica is used as the bottom cladding (n = 1.444 at 1550 nm) and air is used as top cladding(n = 1.0). The above conditions and components were integrated into a single-mode waveguide, with an effective refractive index for the fundamental transverse electric (TE) mode given by n_{eff} = 1.471. Using the effective index, we can calculate the grating period using the Bragg Equation 1 given below:

$$\lambda_B = 2 * n_{eff} * \Lambda \quad (1)$$

where λ_B is the Bragg wavelength, n_{eff} the effective refractive index of the fundamental TE mode, and Λ the grating period.

The grating region comprises two grating sections with widths equal to w + Δw, and w−Δw, with each section having effective indices n_{eff1} and n_{eff2}, respectively, and periodicity, N. Due to the large index contrast, a broad reflection spectrum is expected. This grating was designed to afford a broad reflection spectrum with a central transmission peak with narrow linewidth and high transmission, which can be accomplished by adding a

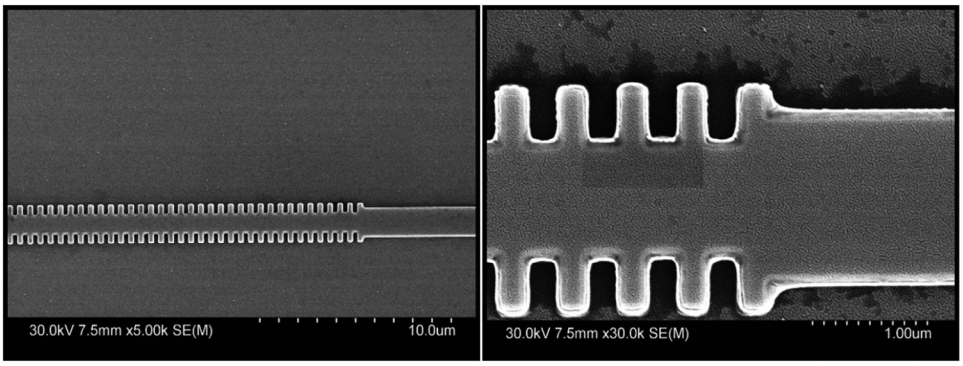

Figure 2. SEM images of the representative fabricated phase-shifted Bragg grating from poly(S-*r*-DIB) with a period (N = 400) and dimensions (w = 1.5 μm; Δw = 250 nm) in close agreement with the designed device dimensions from Figure 1.

quarter-wave phase shift in the center of the grating. The phase shift was achieved by adding an extra section in the center with a length equal to a single period Λ and width $w + \Delta w$ (Figure 1a). The total length of the grating region is (2N+1) × Λ. Figure 1 shows the structure of the PSBG, along with the transmission spectrum for various values of *N*. The EME modeling of this grating with grating ranging N = 200–400 afford progressively sharper Bragg peaks with varying corrugation widths (Δw = 100 vs 250 nm; Figure 1b,c respectively). The observed behavior is consistent with basic coupled mode theory considerations, where we expect that the contrast of the filter will be enhanced by both longer gratings and larger refractive index modulation, while the bandwidth of features will generally narrow with increasing length.

2. Lithographic Fabrication of Poly(S-*r*-DIB) Bragg Gratings

The Phase Bragg gratings were fabricated through a series of conventional lithographic processes using poly(S-*r*-DIB) (70-wt% sulfur copolymer composition, $n \approx 1.75$). The devices were fabricated on silicon wafers with a thermally evaporated 6 μm thick silicon dioxide (SiO_2) cladding layer, where the thickness of the SiO_2 layer was sufficient to isolate the guided light from the high-index silicon substrate. The substrate is cleaned with acetone/isopropyl alcohol (IPA) followed by 2 min of oxygen plasma cleaning to remove any organic impurities. A *CHIPs* poly(S-r-DIB) solution (c = 350 mg mL^{-1} in chlorobenzene) was spin-coated onto solvent and O_2 plasma cleaned substrates and baked to afford a 450 nm thick film. A layer of the e-beam resist maN2403 was then spin-coated on top of the poly(S-*r*-DIB) film to yield a 275 nm thick film for subsequent e-beam patterning. The grating pattern was then generated by e-beam exposure of the sample using the Elionix EBL system with an optimized dose of 450μC cm^{-2}, followed by development in resist developer, maD525 (45–60 s). Finally, the device was dry-etched using the Plasmatherm reactive ion etcher (RIE) tool to transfer the pattern to the *CHIPs* poly(S-*r*-DIB). The etching recipe has been optimized for poly(S-*r*-DIB) *CHIPs* to yield low etch roughness and minimal sidewall scattering losses as we previously demonstrated for waveguiding photonic devices.[13] Successful fabrication of the poly(S-*r*-DIB) Bragg grating was morphologically and dimensionally confirmed by scanning electron microscopy (SEM). A representative poly(S-*r*-DIB) grating with a period of N = *400*, the grating width (w = 1.5 μm), and corrugation width (Δw = 250 nm) are shown in **Figure 2**.

2.1. Optical Characterization of Phase-Shifted Bragg Gratings

We have established a comprehensive testing capability for both passive and active photonic integrated circuits; this includes a variety of light sources (tunable lasers, superluminescent diodes, erbium-doped fiber amplified spontaneous emission sources), six-axis with angle control of input/output fiber position, infrared cameras for observing waveguide modes, optical spectrum analyzers, and thermoelectric devices for control of chip temperature, among other capabilities. For grating optical characterization, we used a superluminescent diode (SLD) source from Inphenix, Inc., which has broadband transmission from 1460 to 1560 nm (Figure 4a). The input light is launched using SMF28 optical fiber and is coupled into the waveguide via end-fire coupling. Polarization paddles were attached at the input to adjust the polarization during characterization, where the polarization was set to TE and attain maximum lateral confinement of the optical mode in the waveguide. Based on the simulation of the waveguide cross-section, the confinement factor is estimated to be 0.62, while the effective index was 1.471 and the group index was 1.717 for the fundamental TE mode. The output light was collected by another SMF28 fiber well-aligned to attain maximum coupling. The characterization setup is shown in **Figure 3**, along with the waveguide mode in the inset. The total fiber-to-fiber insertion loss of the waveguide away from the Bragg region was measured to be 15 ± 2 dB using this apparatus. As the waveguide width corrugation increased (Δw = 100–250 nm), the insertion loss decreased by 5 dB. Waveguide gratings with varying corrugation widths and grating periods were sequentially characterized, and the output spectrum was monitored using the Yokogawa AQ6321B optical spectrum analyzer (OSA). We observed that for the waveguide with Δw = 100 nm, the Bragg peak shape sharpened and its amplitude grew as the number of grating periods increased from 200 to 400. The peaks were further strengthened for the waveguide with Δw = 250 nm for 200 and 300-period gratings. For the device with Δw = 250 nm and N = 300, corresponding to a total grating length of 312 μm, the central

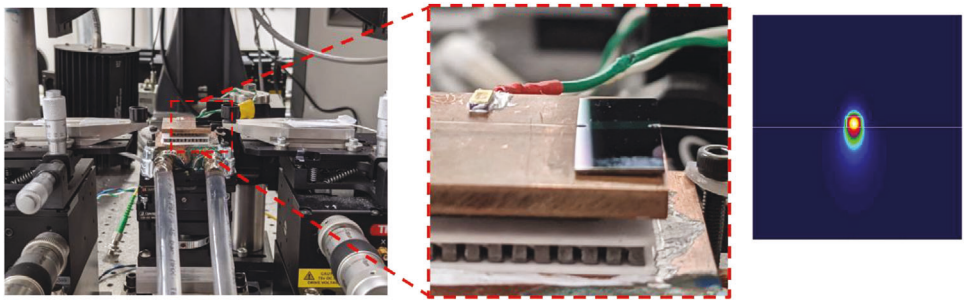

Figure 3. Experimental apparatus for phase-shifted Bragg grating with a sample sitting on temperature-controlled stage, input and output fibers are edge coupled to the chip and pigtailed to eliminate any thermal drift. The simulated mode profile is shown in the top right figure.

phase-shifted Bragg peak has a full-width half maximum (FWHM) of 0.4 nm and reflection bandwidth of 10 nm. The characterization results are summarized in **Figure** 4b,c.

2.2. Results and Analysis of Phase-Shifted Bragg Gratings

An attractive feature of the PSBG photonic transfer characteristic is the sensitivity of the defect mode transmission to external stimuli and environmental conditions, which enables the mapping of transmission profiles with varying conditions, such as temperature and pressure.[15–19] Hence, tracking of transmission peak shifts with temperature affords direct information on fabricated polymer thermal properties, in this case, the glass transition of poly(S-*r*-DIB) as a nanostructured, supported thin film *in operando* as an integrated photonic element. It is particularly useful to report on TO properties that are more important for integrated photonic device performance evaluation versus simple bulk glass transition values.[18] As seen in **Figure** 5b, the Bragg transmission peak shifts linearly between the temperature range of 5–40 °C with a constant slope and shifts linearly again between 40 and 95 °C with a different slope. As the Bragg peak is primarily dependent on the effective index of the waveguide and the grating pitch, we can analyze the thermal shift of the Bragg peak by considering the TO effect and the thermal expansion of the grating dimensions. Furthermore, the inflection of the Bragg peak versus temperature in the poly(S-*r*-DIB) PSBG arises from the glass transition assignable at T = 40 °C for this 70-wt% sulfur copolymer of poly(S-*r*-DIB). This value was in better agreement with the T_g of this sulfur copolymer as estimated by dynamic mechanic analysis (DMA) which exhibited a slower and more comparable heating rate of 3 °C min^{-1} [20] versus the much lower T_g value measured using DSC (T_g = 9.9–16 °C) at faster rates of heating (10–15 °C min^{-1}).[9,20] Analyzing and separating the impact of both will provide an accurate TOC for the polymer. It should be noted that the measured glass transition temperature of polymers generally varies with the rate of temperature change applied and hence it is important to wait for the sample to reach equilibrium before measurements are made. While making the measurements, the stage temperature was slowly increased at a rate of 5 °C min^{-1}. Once the stage reaches the setpoint temperature, the temperature is maintained for 2 min before recording the transmission spectrum. The transmitted power and the spectrum were monitored and the data was time-averaged to ensure stability. The waveguide device consists of a silicon substrate, silica bottom cladding, poly(S-*r*-DIB) core, and no top cladding. For the extraction of TOC, we need to first separate the wavelength shift due to a change in the effective index from that due to the thermal expansion of materials. Silicon and silica both have very low coefficients of thermal expansion (CTE);[1] hence their expansion will not affect the Bragg peak. As the silicon substrate constrains the polymer, only polymer expansion out of the plane is possible, which we ignore in this discussion. We consider the Bragg peak shift to be principally due to the TO change in the refractive index of the core (CHIPs) and cladding (SiO_2) materials. This can be estimated by first calculating the temperature dependence of the Bragg peak. Figure 5b plots the Bragg peak

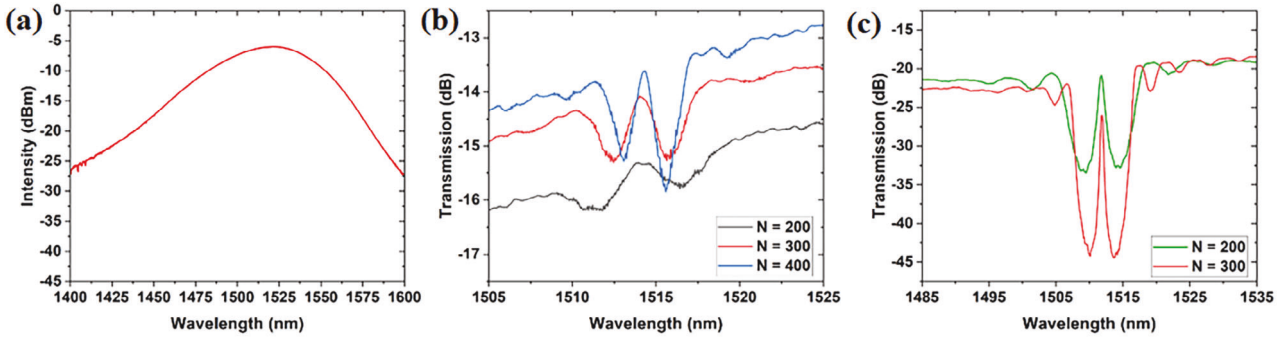

Figure 4. a) The output spectrum of the SLD source is shown as obtained by the OSA. b) The transmission spectra for gratings with 100 nm corrugation and periodicity, *N* varying between 200, 300, and 400 periods. c) The spectra of the transmission gratings with 250 nm corrugation and periodicity, *N* varying between 200 and 300 periods. For the case with 400 periods and 250 nm corrugation width, the OSA spectrum was below the noise floor and, hence, not shown.

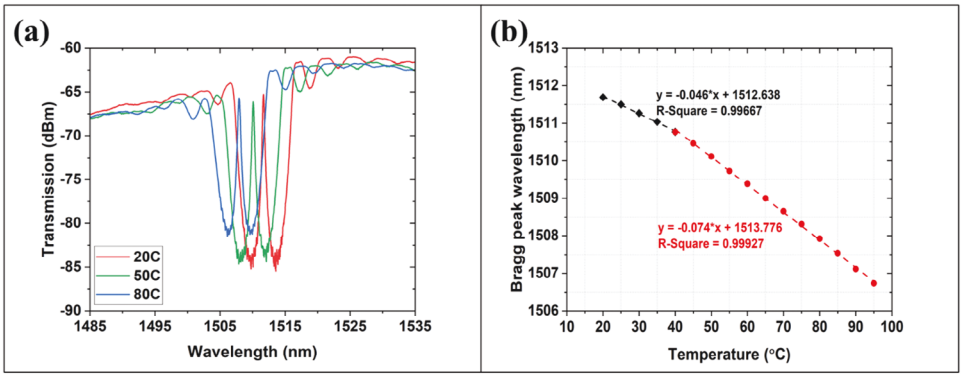

Figure 5. a) Transmission spectrum of the grating as measured with the OSA for three different temperature readings. As seen in the figure, the spectrum is blue-shifted as the temperature increases, indicating an effective negative TO coefficient for the waveguide. b) Location of the central Bragg peak versus the temperature of the thermal stage. Near 40C, there is a change in the slope of the curve, indicating the glass transition temperature of the optical polymer.

wavelength versus temperature with the data fit to a line, and we can extract $d\lambda_B/dT$ from the fit parameters. Using the Bragg Equation (1) and the designed grating period, we can also calculate the derivative of the effective index, dn_{eff}/dT. While it is not straightforward to extract the TOC of *CHIPs* from the effective index sensitivity, we can provide an estimate. In order to do the calculation, we need to first simulate the waveguide cross-section using an eigenmode solver and obtain an effective index that accurately matches the experimentally measured effective index. Next, using the experimental value of the effective index and the TOC for silica obtained from the literature, we can calculate the required refractive index of poly(S-*r*-DIB) to match the experimentally measured effective index.

Repeating these calculations at all temperature measurement points, we can get the change in refractive index versus temperature. Linearly fitting this data, we can calculate the TOC of the optical polymer. The accuracy of this method depends on the simulation accuracy; hence, it is important to do a mesh refinement and convergence study of the eigenmode solution. We used Fimmwave (Photon Design) to make the calculations. Following the procedure described above, the TOC of the polymer is found to be -7.8×10^{-5} °C^{-1} between 20 and 40 °C and -1.4×10^{-4} °C^{-1} between 40 and 95 °C. Compared to most commercially available polymers for optical applications, *CHIPs* have one of the lowest TOCs ever measured (**Table 1**). This small TOC value can be attributed to the positive TOC contribution of the unusually high sulfur content in poly(S-r-DIB) (50-wt%) which dramatically mitigates the negative TOC contribution from the organic monomer (DIB) units in the material in an effective medium sense. This suggests that there may be a stoichiometric combination of sulfur and DIB monomer that will result in a polymer with zero TOC which would be an exciting achievement and useful for low-cost thermally stable photonic circuits. Future work is planned to study the dependence of TOC and the zero crossing temperature of CHIPs with respect to the stoichiometric ratio of sulfur and DIB monomer.

Table 1. Thermo-optic coefficient of optical polymers.

Polymer type	Thermo optic coefficient $dn/dT \times 10^{-4}$ [/°C]	Refs.
PMMA	−1.3	[15]
Polycarbonate	−0.9	[15]
Polystyrene	−1.2	[15]
ZEONEX	−1.22	[16]
ZPU	−1.8	[17]
Poly(S-*r*-DIB) *CHIPs* (70-wt% sulfur)	−0.78	This work

The other notable result achieved in this work is the demonstration of the inflection point where the TOC value of the polymer changes. This inflection point can be taken to estimate the T_g of the polymer since the TO effect in polymers derives largely from temperature-dependent volume changes. Sulfur-based polymers have been reported to have dynamic covalent reconfiguration, resulting in significant variation in the measured T_g values using traditional methods, such as differential scanning calorimetry (DSC), dynamic mechanical analysis (DMA), or small amplitude oscillatory shear.[21–23] The Bragg grating technique can be used in such situations to precisely determine the T_g of the polymer.

Furthermore, for novel polymers where it may be difficult to etch gratings, gratings can be made by making trench molds in the silica bottom cladding followed by spin coating of the polymer. These buried channel waveguides will have the advantage of using well-established fabrication processing for silica while maintaining a similar level of measurement accuracy. We suggest this method as a robust and straightforward technique to make precise TO measurements of novel optical polymers. In the future, we will demonstrate a study for a broader range of materials with compelling optical properties, along with the application of nanoimprint methods for photonic device component fabrication, as recently demonstrated with poly(S-*r*-DIB) infrared polarizers.[24]

3. Conclusion

We have demonstrated the first fabrication of phase-shifted Bragg gratings using a novel optical polymer, *CHIPs* from

poly(S-*r*-DIB). We then characterized the gratings to estimate the temperature dependence of the PSBG peak and extracted the TO coefficient of the polymer from the result. The TOC of CHIPs was remarkably lower than all of the current state-of-the-art commodity optical polymers and can be tuned to have different values depending upon the composition of the polymers. Future work would include demonstrations of CHIPs with reduced TOC, measurements of glass transitions of novel optical polymers using this technique, and demonstration of photonic devices that can work over a wide range of temperatures without significant thermal drift.

4. Experimental Section

Synthesis of Poly(S-r-DIB) as the High RI Core Material: The polymer was synthesized using the inverse vulcanization process with a composition of 70-wt% sulfur.[13] In this process, bulk sulfur powder was heated to 185 °C to form liquid sulfur, which was accompanied by a color change of the medium from yellow to red, indicating the conversion of the S_8 ring into liquid sulfur diradical followed by the formation of polymeric sulfur. At this point, a room-temperature aliquot of 1,3-diisopropenylbenzene (DIB) was added to the sulfur mixture, which results in a homogeneous yellow solution of much lower viscosity. After a short period of mixing and cooling at room temperature, the resulting formation was a transparent red polymeric glass indicating the copolymerization of the DIB monomer with sulfur.

Waveuide Fabrication Process: The polymer was spin-coated on a silicon wafer with a 6 µm thick thermally evaporated silicon dioxide layer, which serves as the lower cladding for the waveguide. The oxide layer was thick enough to isolate the light from the higher-index silicon substrate underneath. Poly(S-*r*-DIB) was dissolved in chlorobenzene (350 mg mL^{-1} concentration) at 115 °C for 15 min until no visible particles were observed. The polymer was then left overnight to cool and to allow for any excess unreacted sulfur to precipitate to the bottom of the glass vial. The dissolved solution was then filtered using a 0.2 µm PTFE membrane syringe filter to remove any undissolved particles or any remaining impurities in the solution. Before spin coating, the substrate was cleaned with acetone and isopropanol (IPA), blown dry with nitrogen, and then O_2 plasma cleaned for 2 min to remove any organic impurities and improve the adhesion of the polymer to the surface. The polymer was then spin-coated at 3000 rpm with 500 rpm s^{-1} acceleration for 30 s. The remaining solvent was evaporated by heating the wafer at 110 °C for 5 min; the resulting film was 450 nm thick. The long bake time was necessary for removing any solvent, which improves adhesion, etch resistance, and chemical compatibility. After the wafer cools down to room temperature, the electron beam lithography (EBL) resist maN2403 was spin coated directly on top of the polymer at 4000 rpm with 500 rpm s^{-1} acceleration for 30 s, followed by baking at 95 °C for 1 min resulting in a 275 nm thick resist layer. The photonic circuit was then written using an Elionix EBL system with an optimized dose of 450 µC cm^{-2}. Once the e-beam exposure was completed, the exposed pattern was developed in the maD525 developer for 45–60 s. To transfer the pattern from the resist onto the polymer, the sample was etched using a fluorine-oxygen-argon etch in an inductively coupled plasma etcher (Plasmatherm ICP RIE). The etching recipe was specifically designed for the CHIPs family of polymers and comprises a mixture of CHF_3, O_2, and Ar gases. CHF_3 creates fluoride radicals which remove the sulfur molecules, while O_2 etches the organic part of the polymer, and Ar makes the etching anisotropic resulting in vertical sidewalls. RF and ICP power were also optimized to control the etch rate, and sidewall roughness, and reduce redeposition (grass formation) on the substrate. The bottom silicon dioxide cladding layer has a much lower etch rate than the polymer for this etching recipe and acts as an etch stop to signal the etch's completion. The resulting etch rate of CHIPs was 312 nm min^{-1}, and the etch rate of maN2403 was 192 nm min^{-1}; hence the resist can act as an effective etch mask. The thicknesses of the polymer and resist layers were optimized to ensure that the resist was fully etched away while the polymer was through etched. Any remaining resist can be removed by rinsing the sample with acetone/IPA. The etched waveguides have smooth sidewalls and ≈90° sidewall angles. The high quality of the fabricated devices was shown in Figure 2. The final fabricated device was prepared for optical characterization by cleaving the end facets with a diamond scribe. The waveguides can be accessed after cleaving and easily butt coupled to an optical fiber to launch the input light and collect the output light.

Optical Characterization Setup for Testing Photonic Devices: Grating optical characterization was done with a superluminescent diode (SLD) source from Inphenix, Inc., which has broadband transmission from 1460 to 1560 nm. The input light was launched using SMF28 optical fiber and was coupled into the waveguide via end-fire coupling. Polarization paddles were attached to the input to adjust the polarization during characterization. The polarization was set to TE to attain maximum lateral confinement of the optical mode in the waveguide. Based on the simulation of the waveguide cross-section, the confinement factor was estimated to be 0.62, while the effective index was 1.471 and the group index was 1.717 for the fundamental TE mode. The output light was collected by another SMF28 fiber that was well-aligned to attain maximum coupling. The characterization setup was shown in Figure 3, along with the waveguide mode. The waveguide's total fiber-to-fiber insertion loss away from the Bragg region was 15 ± 2 dB. As the waveguide width corrugation increases from 100 to 250 nm, the insertion loss also decreases by 5 dB. Waveguide gratings with varying corrugation widths and grating periods were sequentially characterized and the output spectrum was monitored using a Yokogawa AQ6321B optical spectrum analyzer (OSA). It was observed that for the waveguide with $\Delta w = 0.1$ µm, the Bragg peak sharpened and strengthened as the number of grating periods increased from 200 to 400. The peaks were further strengthened for the waveguide with $\Delta w = 0.25$ µm for 200 and 300-period gratings. For the device with $\Delta w = 0.25$ µm and N = 300, corresponding to the total grating length of 312 µm, the central phase-shifted Bragg peak has a full-width half maximum (FWHM) of 0.4 nm and reflection bandwidth of 10 nm.

Thermo-Optic Coefficient Measurement: The temperature-dependent position of the Bragg peak was measured where fabricated gratings were kept on a copper thermal stage fitted with water-cooled heatsinks and an Arroyo thermoelectric cooler (TEC) stage underneath the sample stage. The stage temperature was monitored using a Texas Instruments temperature sensor, which sends a feedback signal to the Arroyo controller and helps maintain a stable temperature. The water-cooling system rapidly cools the stage while minimizing any vibrations, essential for fiber-to-fiber end-fire coupling. The sample was fixed on the sample stage with the help of thermally conductive tape, and the input and output fibers were aligned to the end facet of the waveguide until the maximum coupling was achieved. After the initial alignment, the output spectrum was monitored using the Yokogawa OSA, and the location of the central Bragg peak was extracted from the output spectrum. The sample was ramped down from room temperature to 20 °C in steps of 5 °C min^{-1}. The system was stabilized at the set temperature for each data point, and the corresponding Bragg peak was recorded. The sample was then slowly heated from 20 to 90 °C in the steps of 5 °C min^{-1}. As the temperature of the stage was increased, the output power was also monitored using a power meter. The output power remained within ± 2 dB while the temperature was varied. Figure 4 above shows the results of the thermal characterization.

Acknowledgements

The authors acknowledge the National Science Foundation (PFI-RP 1940942, MRI-1920234, DMREF-2118578, CHE-1807395, MRI-ECCS-1725571), the Air Force Research Laboratories (FA8650-16-D-5404), the RII Research Advancement Grant program, and the Hitachi Electron Microscopy scholarship for support of this work.

Conflict of Interest

R. A. Norwood is an owner and officer of Norcon Technologies Holding Inc. with which a financial conflict of interest exists.

Data Availability Statement

The data that support the findings of this study are available from the corresponding author upon reasonable request.

Keywords

Bragg grating, chalcogenides, CHIPs, integrated photonics, optical polymers, thermo-optic coefficient

Received: May 11, 2024
Revised: June 6, 2024
Published online:

[1] H. Zuo, S. Yu, T. Gu, J. L. L. Hu, *Opt. Express* **2019**, *27*, 11152.
[2] A. V. Shneidman, K. P. Becker, M. A. Lukas, N. Torgerson, C. Wang, O. Reshef, M. J. Burek, K. Paul, J. McLellan, M. Lončar, *ACS Photonics* **2018**, *5*, 1839.
[3] M. Rezem, A. Gunther, B. Roth, E. Reithmeier, M. Rahlves, *J. Lightwave Technol.* **2017**, *35*, 299.
[4] R. Dangel, A. La Porta, D. Jubin, F. Horst, N. Meier, M. Seifried, B. J. Offrein, *IEEE J. Sel. Top. Quantum Electron.* **2018**, *24*, 1.
[5] J. Xiong, E. L. Hsiang, Z. He, T. Zhan, S. T. Wu, *Light: Sci.Appl.* **2021**, *10*, 1.
[6] A. Shishido, *Polym. J.* **2010**, *42*, 525.
[7] Y. Li, J. Ibanez-Guzman, *IEEE Signal Processing Magazine* **2020**, *34*, 50.
[8] J. Matsui, K. Akamatsu, N. Hara, D. Miyoshi, H. Nawafune, K. Tamaki, N. Sugimoto, *Anal. Chem.* **2005**, *77*, 4282.
[9] W. J. Chung, J. J. Griebel, E. T. Kim, H. Yoon, A. G. Simmonds, H. J. Ji, P. T. Dirlam, R. S. Glass, J. J. Wie, N. A. Nguyen, B. W. Guralnick, J. Park, Á. Somogyi, P. Theato, M. E. Mackay, Y. E. Sung, K. Char, J. Pyun, *Nat. Chem.* **2013**, *5*, 518.
[10] J. J. Griebel, S. Namnabat, E. T. Kim, R. Himmelhuber, D. H. Moronta, W. J. Chung, A. G. Simmonds, K. J. Kim, J. Van Der Laan, N. A. Nguyen, E. L. Dereniak, M. E. MacKay, K. Char, R. S. Glass, R. A. Norwood, J. Pyun, *Adv. Mater.* **2014**, *26*, 3014.
[11] T. S. Kleine, L. R. Diaz, K. M. Konopka, L. E. Anderson, N. G. Pavlopolous, N. P. Lyons, E. T. Kim, Y. Kim, R. S. Glass, K. Char, R. A. Norwood, J. Pyun, *ACS Macro Lett.* **2018**, *7*, 875.
[12] L. E. Anderson, T. S. Kleine, Y. Zhang, D. D. Phan, S. Namnabat, E. A. LaVilla, K. M. Konopka, L. Ruiz Diaz, M. S. Manchester, J. Schwiegerling, R. S. Glass, M. E. Mackay, K. Char, R. A. Norwood, J. Pyun, *ACS Macro Lett.* **2017**, *6*, 500.
[13] A. Nishant, K. Kim, S. Showghi, R. Himmelhuber, T. S. Kleine, T. Lee, J. Pyun, *Adv. Opt. Mater.* **2022**, *10*, 2200176.
[14] C. Husko, A. Ducharme, N. M. Fahrenkopf, J. R. Guest, *OSA Continuum* **2021**, *4*, 933.
[15] J. Komma, C. Schwarz, G. Hofmann, D. Heinert, R. Nawrodt, *Appl. Phys. Lett.* **2012**, *101*, 041905.
[16] Z. Zhang, P. Zhao, P. Lin, F. Sun, *polymer commun.* **2006**, *47*, 4893.
[17] S. N. Kasarova, N. G. Sultanova, I. D. Nikolov, *J. Phys: Conf. Ser.* **2010**, *253*, 012028.
[18] L. Eldada, R. Blomquist, M. Maxfield, D. Pant, G. Boudoughian, C. Poga, *IEEE Photonics Technol. Lett.* **1999**, *11*, 448.
[19] M. Rosenberger, S. Hessler, S. Belle, B. Schmauss, R. Hellmann., *Opt. Express* **2014**, *22*, 5483.
[20] T. S. Kleine, N. Nguyen, L. E. Anderson, S. Namnabhat, E. A. LaVilla, S. A. Showghi, P. T. Dirlam, C. B. Arrington, M. A. Manchester, J. Schwiegerling, R. S. Glass, K. Char, R. A. Norwood, M. E. Mackay, J. Pyun, *ACS Macro Lett.* **2016**, *5*, 1152.
[21] J. J. Griebel, N. Ngyugen, A. Astashkin, R. S. Glass, M. E. Mackay, K. Char, J. Pyun, *ACS Macro Lett.* **2014**, *3*, 862.
[22] J. J. Griebel, N. Ngoc, S. Namnabat, L. E. M. Anderson, M. E., K. G. Char, R. S., R. A. Norwood, J. Pyun, *ACS Macro Lett.* **2015**, *4*, 862.
[23] D. J. Bischoff, T. Lee, K. S. Kang, J. Molineux, W. O. Parker, J. Pyun, M. E. Mackay, *Nat. Commun.* **2023**, *14*, 7553.
[24] W. Cho, J. Hwang, S. Y. Lee, J. Park, N. Han, C. H. Lee, S.-W. Kang, A. Urbas, J. O. Kim, Z. Ku, J. J. Wie, *Adv. Mater.* **2023**, *35*, 2209377.

